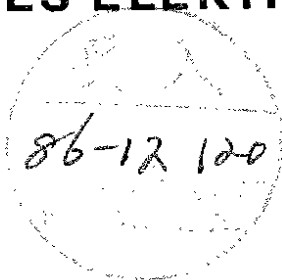


DESY 86-117
September 1986



REVIEW OF THE EXPERIMENTAL PARALLEL SESSIONS

by

J.H. Field

Deutsches Elektronen-Synchrotron DESY, Hamburg

ISSN 0418-9833

NOTKESTRASSE 85 · 2 HAMBURG 52

DESY behält sich alle Rechte für den Fall der Schutzrechtserteilung und für die wirtschaftliche Verwertung der in diesem Bericht enthaltenen Informationen vor.

DESY reserves all rights for commercial use of information included in this report, especially in case of filing application for or grant of patents.

To be sure that your preprints are promptly included in the
HIGH ENERGY PHYSICS INDEX ,
send them to the following address (if possible by air mail) :

DESY
Bibliothek
Notkestrasse 85
2 Hamburg 52
Germany

The 9 short talks presented in the experimental parallel sessions may be grouped according to subject as:

RESONANCE PRODUCTION

- J.C. Sens (TPC 2γ) Test of C-conservation in η' decay
- R. Gerhards (TASSO) Measurement of $\Gamma_{\gamma\gamma}(A_2)$
- V. Mertens (TASSO) Measurement of $\Gamma_{\gamma\gamma}(\eta_c)$

EXCLUSIVE PROCESSES

- Z. Ajaltouni (DM2) $\gamma\gamma \rightarrow \pi^+\pi^-$
- C.J. Zeitlin (TPC 2γ) $\gamma\gamma \rightarrow p\bar{p}$
- A. Courau (DELCO) $\gamma\gamma \rightarrow e^+e^-$, $\gamma e \rightarrow \gamma e$ and luminosity monitoring at HERA
- F. Le Diberder (CELLO) $e^+e^- \rightarrow 1\bar{1}1\bar{1}$; $1,1' = e, \mu, \tau$

STRUCTURE FUNCTIONS

- A. Cordier (ALEPH) F_2^{γ} measurement at LEP
- R.R. McNeil (TPC 2) F_2^{γ} measurements at low Q^2

In addition there was a presentation by F. Wormser of the NA14 (CERN) results on deep inelastic Compton scattering. I shall not discuss these as they have been fully covered in the talks of A. Seiden and P. Aurenche.

J.C. Sens

Sens reported new results on exclusive η' production from the TPC 2γ Collaboration. The process observed is:

$$e^+e^- \rightarrow \eta'e^+e^-, \eta' \rightarrow \pi^+\pi^-\gamma$$

320 ± 18 events were obtained, after cuts, for a total integrated luminosity of 75 pb⁻¹. There was no tagging requirement. The $\pi^+\pi^-$ mass spectrum was consistent with 100% $\eta' \rightarrow \rho\gamma$ decay. Using

$$BR(\eta' \rightarrow \rho\gamma) = 0.300 \pm 0.016$$

the radiative width was found to be:

$$\Gamma_{\gamma\gamma}(\eta') = 4.5 \pm 0.3 \text{ (stat.)} \pm 0.6 \text{ (syst.) keV}$$

in good agreement with the world average value¹⁾.

REVIEW OF THE EXPERIMENTAL PARALLEL SESSIONS

J.H. Field
DESY
Notkestrasse 85, 2000 Hamburg 52
GERMANY

Rapporteur talk at the VII International Workshop on Photon-Photon Collisions, Paris, April 1986

An interesting question that can be investigated in the decay $\eta' \rightarrow \pi^+ \pi^- \gamma$ is the conservation of C parity in electromagnetic interactions. After the discovery of CP violation in the decay $K_L \rightarrow \pi^+ \pi^-$ in 1964 Prentki, Veitman, Lee, and Wolfenstein considered the possibility of a semi-strong interaction that would violate C, T and conserve P, S.

Such an interaction could result in a charge asymmetry in the decays $\eta, \eta' \rightarrow \pi^+ \pi^- \gamma, \eta \rightarrow \pi^+ \pi^- \pi^0$. Several experiments were performed in the late sixties to search for such effects, especially in η decays. No significant asymmetries were found within experimental sensitivities of $\approx 0.2\%$. For the η' decay $\eta' \rightarrow \pi^+ \pi^- \gamma$ no charge asymmetry was found within a 1 σ error of $\pm 5\%$. This conclusion is confirmed by the TPC 2 γ data. By comparing the number of events in the $\pi^+ \pi^- \gamma$ Dalitz plot with $T_+ > T_-$ and $T_- > T_+$ a corrected asymmetry of $-1.4 \pm 6.0\%$ is found. This implies that either C is conserved (within the stated error) in the decay, or alternatively that it is completely violated. In the latter case the $\pi^+ \pi^-$ system must be in a D-wave angular momentum state.

Actually the spin of the η' is known to be zero from a comparison of the directly measured width $\Gamma(\eta')^2$ and the experimental value of $\Gamma_{\gamma\gamma}(\eta')/BR(\eta' \rightarrow \gamma\gamma)^3$. The hypothesis of C-conservation (violation) can then be tested by comparing the experimental data with the decay |matrix element|² in the two cases:

$$q^2 k_{\pi\pi}^2 \sin^2 \theta_{\pi\pi} \quad (\text{P-Wave, C-conserving})$$

$$4 q^2 k_{\pi\pi}^2 \sin^2 \theta_{\pi\pi} \cos^2 \theta_{\pi\pi} \quad (\text{D-Wave, C-violating})$$

Here q, k are the momenta of a pion and the decay photon respectively in the $\pi\pi$ rest frame. $\theta_{\pi\pi}$ is the angle between the photon momentum and the momentum of a pion in the same frame. By fitting the distributions of $\theta_{\pi\pi}$ (angle of the decay γ with respect to the incoming $\gamma\gamma$ direction in the η' rest frame), $\theta_{\pi\pi}$ and $m_{\pi\pi}$ the D-wave solution is excluded, so that C is indeed conserved in η' decay. Also, assuming C conservation, spin 2 is excluded for the η' from a fit to the $\theta_{\pi\pi}, \theta_{\pi\pi}, m_{\pi\pi}$ distributions to the appropriate |matrix element|², thus confirming the η' spin determination mentioned above.

R. Gerhards

The TASSO Collaboration has made a new measurement of untagged exclusive A_2 production at $\sqrt{s} = 34$ GeV for an integrated luminosity of

70 pb⁻¹:

$$e^+ e^- \rightarrow A_2 e^+ e^-, A_2 \rightarrow \rho^+ \pi^-, \rho^+ \rightarrow \pi^+ \pi^0, \pi^0 \rightarrow \gamma\gamma$$

The final state detected is therefore $\pi^+ \pi^- \gamma\gamma$. A clean π^0 signal is observed in the $\gamma\gamma$ effective mass spectrum. A kinematical fit is made of $M(\gamma\gamma)$ to $M(\pi^0)$ for all events in the π^0 peak:

$$0.07 < M(\gamma\gamma) < 0.20 \text{ GeV}/c^2.$$

The $\pi^+ \pi^- \pi^0$ mass spectrum obtained is shown in Fig. 1. Inclusive background has been removed by a two dimensional side-band subtraction on the $M(\pi^+ \pi^- \pi^0)$ versus $(p_T^{\text{TOT}})^2$ plot where p_T^{TOT} is the total observed transverse momentum. The data is fit to a two component model consisting of a relativistic Breit-Wigner (Curve A) for the A_2 and a smooth distribution (Curve B) for exclusive $\pi^+ \pi^- \pi^0$ production. The Monte Carlo used to describe the A_2 production and decay convolutes transverse photon flux factors with the production cross-section:

$$\sigma(\gamma\gamma \rightarrow A_2 \rightarrow \rho\pi) = 8\pi(2J+1) \times$$

$$\frac{M^2(A_2) \Gamma_{\gamma\gamma}(A_2) \Gamma_{\rho\pi}(A_2)}{s \frac{\Gamma_{\gamma\gamma}(A_2)^2 + M(A_2)^2}{(M(A_2)^2 - s)^2 + M(A_2)^2} \Gamma(A_2)^2}$$

The decay $A_2 \rightarrow \rho\pi$ is described by a $\pi^+ \pi^- \pi^0$ (3 body) phase space factor multiplied by a |matrix element|²:

$$|M|^2 = |BW(\rho^+) \psi(\rho^+, \pi^-) + BW(\rho^-) \psi(\rho^-, \pi^+)|^2$$

BW(ρ) is a Breit-Wigner amplitude for $\rho \rightarrow \pi\pi$ decay:

$$BW(\rho) = \frac{[\Gamma(\rho) \Gamma(\rho) M(\pi\pi)] / P(\rho)]^{1/2}}{M(\rho)^2 - M(\pi\pi)^2 - i\Gamma(\rho) \Gamma(\rho)}$$

while $\psi(\rho, \pi)$ describes the cascade decay $A_2 \rightarrow \rho\pi$ (angles $\theta_{\rho}, \phi_{\rho}$) $\rho \rightarrow \pi\pi$

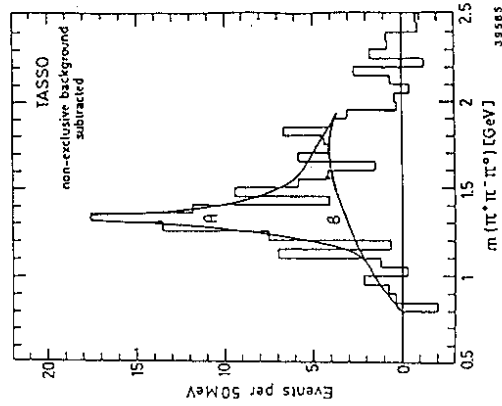


Fig. 1: $\pi^+ \pi^- \pi^0$ effective mass distribution after subtraction of non-exclusive background. Curve A: Breit Wigner fit to A_2 peak (see text). Curve B: estimation of exclusive (non A_2) $\pi^+ \pi^- \pi^0$ contribution (TASSO)

(angles θ_π, φ_π):

$$\psi(\rho, \pi) = \int_{\vec{j}_3} C(j, \vec{j}_3 | L, \vec{j}_3 - \vec{j}_3; j, \vec{j}_3) \times \int_{\theta_\rho, \varphi_\rho} \int_{\theta_\pi, \varphi_\pi} Y_{\vec{j}_3}^j(\theta_\rho, \varphi_\rho) Y_{\vec{j}_3}^j(\theta_\pi, \varphi_\pi)$$

The number of events in the fitted A_2 peak is 55 ± 16 leading to a measured radiative width:

$$\Gamma_{\gamma\gamma}(A_2) = 0.90 \pm 0.27 \text{ (stat.)} \pm 0.16 \text{ (syst.) keV}$$

The updated world average value¹⁾ is:

$$\Gamma_{\gamma\gamma}(A_2) = 0.95 \pm 0.19 \text{ keV}$$

This may be compared with a theoretical expectation of 1.08 ± 0.07 keV using as input the world average value of $\Gamma_{\gamma\gamma}(f)$ and assuming ideal mixing for f, f' and fractional quark charges.

Finally it should be remarked that this experiment gives evidence for significant non-resonant exclusive production of $\pi^+\pi^-\pi^0$ (Curve B in Fig. 1). 3 body phase space was assumed for the Monte Carlo simulation of this contribution.

V. Mertens

A search has been made using the TASSO detector at PETRA for untagged exclusive η_c production via the process:

$$e^+e^- \rightarrow \eta_c e^+e^-, \eta_c \rightarrow K_S^0 K^{\pm} \pi^{\mp}$$

A total integral luminosity of 83.3 pb^{-1} at high energy ($\sqrt{s} > 34 \text{ GeV}$) was used.

The first step in the analysis was to search for a $K_S^0 \rightarrow \pi^+\pi^-$ decay vertex clearly separated from the production vertex in events with 4 charged (2+ve, 2-ve) tracks. The vertex search was performed in the transverse ($R\phi$) plane. Denoting by IP, SV the primary interaction vertex and secondary decay vertex respectively, l is the projected distance between IP, SV and α is the angle between the line joining IP, SV and the direction of the transverse momentum of the K_S^0 candidate (2 per event as K^\pm are not distinguished from π^\pm in this analysis). Also $d_{0,1}, d_{0,2}$ are the projected

distances of closest approach of the two candidate K_S^0 decay pion tracks from IP.

By making suitable cuts on the vertex parameters defined above:

$$\begin{aligned} l &> 0.4 \text{ cm} \\ d_{0,1}, d_{0,2} &> 0.0 \text{ cm} \\ \alpha &< 3^\circ \end{aligned}$$

a clean K_S^0 signal with ≈ 500 events in the peak is observed. Making additional cuts to ensure that only one (+, -) mass combination per event is consistent with K_S^0 :

$$|M(V^0) - M(K_S^0)| < 30 \text{ MeV}/c^2$$

$$|M(34) - M(K_S^0)| > 70 \text{ MeV}/c^2$$

$$[M(V_0) = M(12)]$$

and that $p_T^{\text{TOT}} < 250 \text{ MeV}/c$ (to avoid inclusive backgrounds) the $K_S^0 K^{\pm} \pi^{\mp}$ mass distribution (2 combinations per event, corresponding to $K^+\pi^-, K^-\pi^+$) is shown in Fig. 2. A suggestive peak containing 6.6 ± 3.3 events is seen at the η_c mass. The mass resolution at the peak is estimated to be $60 \text{ MeV}/c^2$.

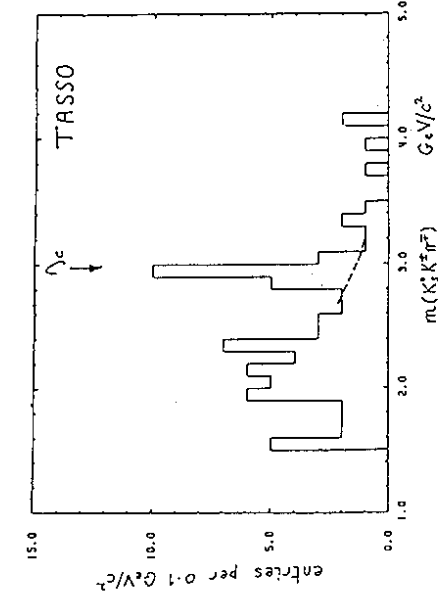


Fig. 2: $M(K_S^0 K^{\pm} \pi^{\mp})$ distribution (2 entries per event) See text for details of cuts (TASSO)

For comparison the published⁴⁾ PLUTO $K_S^0 K^{\pm} \pi^{\mp}$ mass distribution is shown in Fig. 3. The level of background under the η_c peak is lower in the PLUTO data, where there also seems to be evidence for $f' \rightarrow K_S^0 K^{\pm} \pi^{\mp}$ at lower masses.

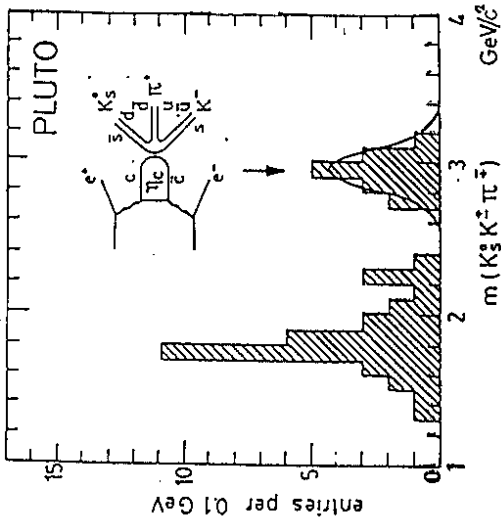


Fig. 3: $M(K_S^0 K_S^0 \pi^+ \pi^-)$ distribution (2 entries per event) (PLUTO, Ref(4))

For the radiative width the two experiments find:

$$\Gamma_{\gamma\gamma}(\eta_c)BR(\eta_c \rightarrow K_S^0 K_S^0 \pi^+ \pi^-) = 1.2 \pm 0.6 \text{ (stat.)} \pm 0.4 \text{ (syst.) keV (TASSO)}$$

$$= 0.5 \pm 0.2 \text{ (stat.)} \pm 0.1 \text{ (syst.) keV (PLUTO)}$$

Combining the MARK III measurement of the product branching ratio: $BR(J/\psi \rightarrow \eta_c \gamma)BR(\eta_c \rightarrow K\bar{K}\pi)$ with the Crystal Ball measurement of $BR(J/\psi \rightarrow \eta_c \gamma)$ gives:

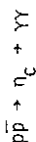
$$BR(\eta_c \rightarrow K\bar{K}\pi) = 6.1 \pm 2.2\%$$

giving for $\Gamma_{\gamma\gamma}(\eta_c)$:

$$\Gamma_{\gamma\gamma}(\eta_c) = 59 \pm 41 \text{ keV (TASSO)}$$

$$= 25 \pm 14 \text{ keV (PLUTO)}$$

These results seem to be at variance both with the ISR experiment⁵⁾ using a gas jet target and a \bar{p} beam to detect:



(which gives a 2σ upper limit of < 7 keV) and with theoretical predictions using the quarkonium annihilation model which suggest $\Gamma_{\gamma\gamma}(\eta_c) \approx 5-6$ keV.

Also, as pointed out by Falvard⁶⁾, if $\Gamma_{\gamma\gamma}(\eta_c)$ were indeed as high as 50 keV the DM2 detector should have observed the direct decay $\eta_c \rightarrow \gamma\gamma$ via the product branching ratio $BR(J/\psi \rightarrow \eta_c \gamma)BR(\eta_c \rightarrow \gamma\gamma)$ and in fact no such signal has been seen.

The errors quoted above on $\Gamma_{\gamma\gamma}(\eta_c)$ seem to be comfortably large, so at first sight there might seem to be no problem, as both values of $\Gamma_{\gamma\gamma}(\eta_c)$ are $< 2\sigma$ from zero. Suppose however that $\Gamma_{\gamma\gamma}(\eta_c)$ is indeed 7 keV, then TASSO (PLUTO) should have observed 0.83 (1.96) events in the η_c peak. They in fact observe 6 (7) events corresponding to Poisson probabilities of 2×10^{-4} (3×10^{-3}). If the large value of $\Gamma_{\gamma\gamma}(\eta_c)$ seen by PLUTO and TASSO is confirmed the conventional quark model theory of radiative widths could be in serious difficulties.

Z. Ajjalouni

The processes:

$$e^+e^- \rightarrow (e^+e^-, \mu^+\mu^-, \pi^+\pi^-) e^+e^-$$

have been investigated at the DCI e^+e^- collider at Orsay using the DM2 detector. The e^+e^- collision energy was in the range:

$$1.38 < \sqrt{s} < 1.88 \text{ GeV}$$

and the integrated luminosity was 530 nb^{-1} . Single or double tag events with two charged tracks of opposite sign are selected.

Because of the low visible energy of the events kinematic separation of e, μ, π pairs is possible. If the energy E_1 of one of the scattered electrons is measured in the tagging system, the energy of the unobserved electron E_2 can be found from overall momentum conservation (only the untagged electron is not observed). The total energy of the pair, $E_{\gamma\gamma}$ is then given by:

$$E_{\gamma\gamma} = \sqrt{s} - E_1 - E_2$$

The common mass m_x of the pair particles is then given by:

$$m_x^2 = [(E_{\gamma\gamma}^2 + \vec{p}_1^2 - \vec{p}_2^2) / (2E_{\gamma\gamma})]^2 - \vec{p}_1^2$$

where \vec{p}_1, \vec{p}_2 are the vector momenta of the two observed tracks. For double tag events the kinematics is overconstrained and allowance can be made for a single photon radiated in the initial state parallel to the beams. The

m_x^2 distribution for the sum of single and double tag events is shown in Fig. 4. The solid curve is a fit to the e, μ peaks taking into account the experimental resolution. A $\pi\pi$ -pair signal is seen above the resolution tail of the lepton pairs. The $\pi\pi$ mass distribution after subtracting leptonic background is shown in Fig. 5. A sharp mass peak is observed around $M(\pi\pi) = 400 \text{ MeV}/c^2$. This can be explained neither by a $\pi^+\pi^-$ Born term, nor the Born term plus a wide ϵ resonance ($M(\epsilon) = 530 \text{ MeV}$, $\Gamma(\epsilon) = 780 \text{ MeV}$) (see Fig. 5). Messier concluded in a talk in the theory parallel session⁷ that conventional theory with $\pi\pi$ phase shifts satisfying current algebra constraints at threshold is not able to explain the enhancement.

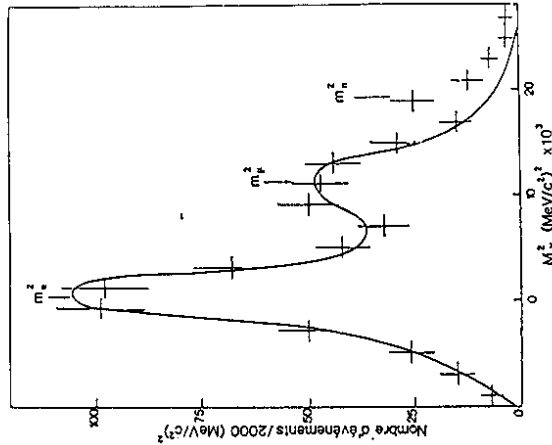


Fig. 4: Distribution of reconstructed $(\text{mass})^2$ of pair particles in the DM2 detector at DCI. Single and double tag events are added.

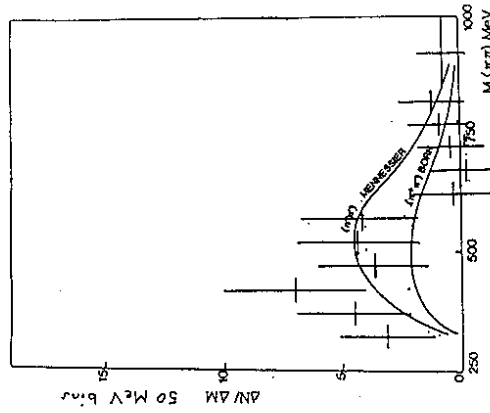


Fig. 5: $M(\pi\pi)$ distribution after subtraction of leptonic background (DM2 detector at DCI), compared to two theoretical predictions. For curve labelled 'Messier' see text.

C.J. Zeitlin

The TPC 2γ Collaboration has studied the process:



in the mass range $2.0 < W_{\gamma\gamma} < 2.8 \text{ GeV}/c^2$. After making vertex and production angle cuts, demanding two oppositely charged tracks, and rejecting e, μ, π, K by χ^2 cuts using the TPC dE/dX information, the p (Fig. 6a) and \bar{p} (Fig. 6b) candidates give clear signals on a dE/dX versus $\log(p)$ plot. The \bar{p} spectrum extends to lower momenta than p . This is due to trigger bias. Annihilation products to \bar{p} which stop in the coil still give a valid trigger. Protons of comparable momentum are ranged out and give no trigger. A very detailed Monte Carlo is needed to correct the acceptance for these differential absorption effects.

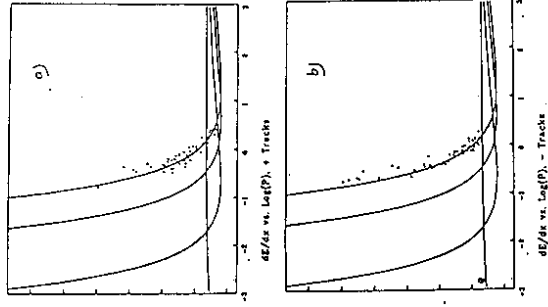


Fig. 6: dE/dX versus $\log(p)$ for $p\bar{p}$ candidates
a) positive tracks
b) negative tracks
(TPC 2γ)

After a visual scan to remove background 39 events remain with $(p_T^{\text{TOT}})^2 < 0.04 \text{ (GeV}/c)^2$. The non-exclusive background is estimated to be $\approx 7\%$ with this p_T^{TOT} cut. A Monte-Carlo simulation is used to relate the observed cross section to the process $\gamma\gamma \rightarrow p\bar{p}$:

$$\frac{d\sigma(e^+e^- \rightarrow p\bar{p}e^+e^-)}{dW_{\gamma\gamma} d|\cos\theta^*|} = \frac{dL_{\gamma\gamma}^{\text{TT}}}{dW_{\gamma\gamma}} \frac{d\sigma(\gamma\gamma \rightarrow p\bar{p})}{d|\cos\theta^*|}$$

where $dL_{\gamma\gamma}^{\text{TT}}/dW$ is the exact luminosity function for transverse photons.

The integrated cross section for $\gamma\gamma \rightarrow p\bar{p}$ for $|\cos\theta^*| < 0.6$ is shown as a function of $W_{\gamma\gamma}$ in Fig. 7. A QCD prediction⁸ lies more than a factor of 10 below the experimental data. Since the experimental data is close to threshold while the QCD prediction should apply in the large

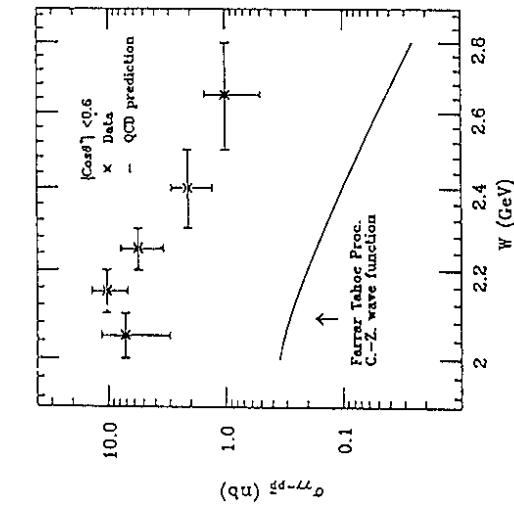


Fig. 7: $\sigma(\gamma\gamma \rightarrow p\bar{p})$ (nb) for $|\cos\theta^*| < 0.6$ compared with a QCD prediction (TPC 2Y)

P_T (perturbative) range, no real conclusion can be drawn from this comparison. The angular distributions for $2.1 < W_{\gamma\gamma} < 2.3$ GeV/c² (Fig. 8a) and $2.3 < W_{\gamma\gamma} < 2.8$ GeV/c² (Fig. 8b) are compared with the same QCD model, but with arbitrary normalisation. The experimental data are consistent with isotropy, unlike the QCD prediction which shows forward peaking, especially in the higher mass interval. Finally it should be remarked that this new TPC 2Y measurement is in good agreement with previously published⁹⁾ TASSO results.

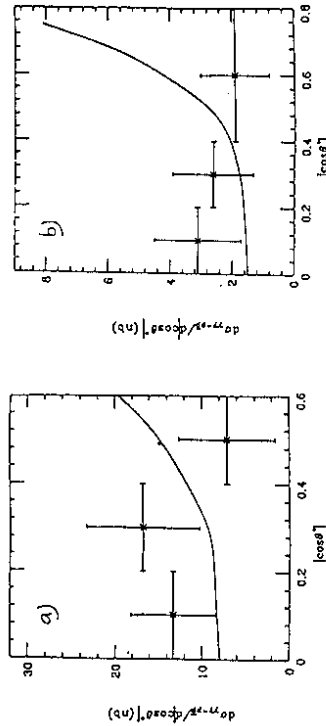


Fig. 8: Angular distributions for $\gamma\gamma \rightarrow p\bar{p}$
 a) $2.1 < W_{\gamma\gamma} < 2.3$ GeV/c²
 b) $2.3 < W_{\gamma\gamma} < 2.8$ GeV/c²
 Curves are a QCD prediction with arbitrary normalisation (TPC 2Y)

A. Courau

The absolute luminosity in e^+e^- colliders is measured using the Bhabha scattering process:

$$e^+e^- \rightarrow e^+e^-$$

A fast relative monitor is provided by small angle scattering where counting rates are high, but the acceptance is poorly known, while large angle scatters with a well defined acceptance (but lower counting rate) provide the absolute monitor. The corresponding elastic scattering process at HERA:

$$ep \rightarrow ep$$

is enormously suppressed at detectable scattering angles by the proton form factor. Other processes must therefore be used for luminosity monitoring.

Courau has suggested¹⁰⁾ to use the QED 2γ collision process:

$$ep \rightarrow l^+l^-ep \quad l = e, \mu$$

The cross section is sufficiently large that lepton pairs at large production angles with an almost back-to-back configuration give a sufficient counting rate for absolute luminosity monitoring. The process is not as 'clean' theoretically as Bhabha scattering due to the sensitivity of the cross section to the elastic and inelastic proton form factors. Such effects can however be minimised by stringent cuts on acoplanarity or total transverse momentum of the produced lepton pair, to ensure that the virtual photons in the process:

$$\gamma^* \gamma^* \rightarrow l^+l^-$$

are almost real.

The cross section in this non-tag case can be accurately estimated using a simple DEPA (Double Equivalent Photon Approximation) model¹¹⁾. Fig. 9 shows the result of a comparison of data from the process:

$$e^+e^- \rightarrow e^+e^-e^+e^-$$

taken in the DELCO detector at PEP with such a model. The agreement is as impressive as the statistical error bars on the data are small!

One disadvantage of this reaction is that a special (low multiplicity charged particle) trigger is needed, and that the events have low visible energy. As background levels (for example from beam gas collisions)

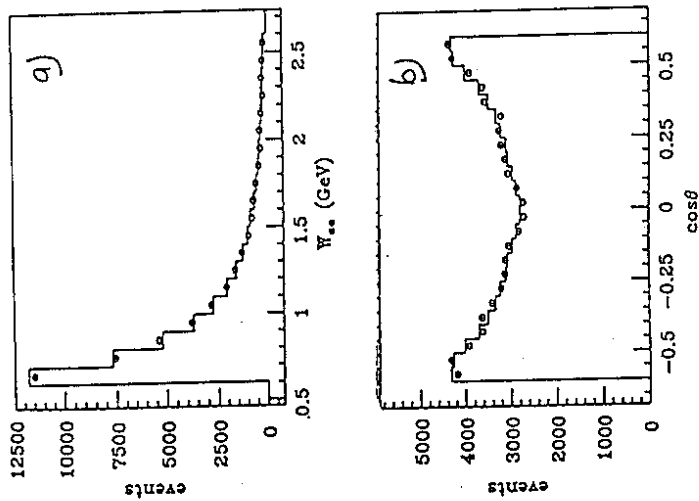


Fig. 9: Comparison of data from the (untagged) process $e^+e^- \rightarrow e^+e^-$ with a DEPA Monte Carlo (histogram).
 a) e^+e^- effective mass
 b) $\cos\theta$ (in the lab.) of e^+, e^- (DELCO)

are expected to be many orders of magnitude higher at HERA than in e^+e^- colliders due to the much higher interaction probability of the proton beam, separation of the process from background may be non-trivial.

Another process, that does not have this disadvantage as it results in a final state of relatively large visible energy, is wide angle beam-beam bremsstrahlung or 'virtual Compton scattering'.¹²⁾

$$e^+ \rightarrow e^+\gamma(p)$$

where the scattered electron and photon are detected at large angle. Such a reaction can be detected by a purely calorimetric trigger, which will anyway be available in all HERA detectors. The distribution of e^+e^- effective mass from the corresponding e^+e^- process:

$$e^+e^- \rightarrow e^+\gamma(e^-)$$

as observed by the CELLO detector¹³⁾ is shown in Fig. 10. Some partial cross sections (in pb) for the process at HERA are ($\theta = 0$ is parallel to the proton beam):

θ_e	$\theta_e = 8 - 30^\circ$	$\theta_e = 30 - 150^\circ$	$\theta_e = 150 - 172^\circ$	$\theta_e = 8 - 172^\circ$
$\theta_Y = 8 - 30^\circ$	0	0.1	1	1
$\theta_Y = 30 - 150^\circ$.4	10	18	28
$\theta_Y = 150 - 172^\circ$	2	49	130	181
$\theta_Y = 8 - 172^\circ$	2	59	149	210

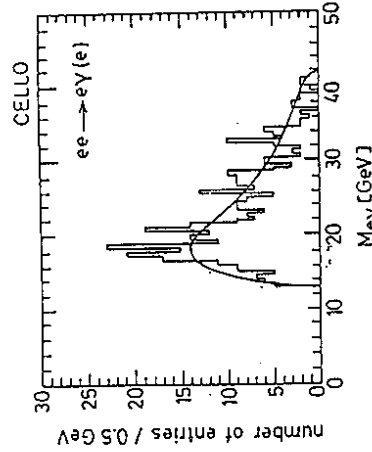


Fig. 10: e^+e^- effective mass distribution from the process: $e^+e^- \rightarrow e^+\gamma(e^-)$ (CELLO, Ref.113)

As the dominant contribution comes from initial state radiation from the electron beam, small angles relative to the electron beam are favoured. The observed cross section in the angular region $8 - 172^\circ \approx 200$ pb is comparable to that for the $e^+e^- \rightarrow e^+\gamma(e^-)$ process in the 'central' region $30 - 150^\circ$ with $M(e^+e^-) > 1$ GeV/c².

Fig. 11 shows the cross sections for the two proposed luminosity monitoring reactions as a function of visible energy. The $\gamma\gamma(e\gamma)$ processes dominate at low (high) visible energies.

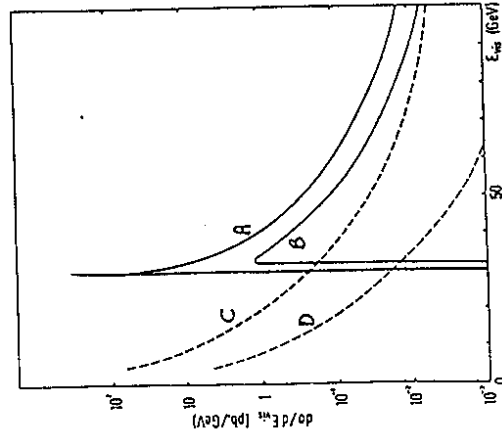


Fig. 11: Cross sections as a function of visible energy for the processes: $e^+e^- \rightarrow e^+\gamma(p)$ (solid lines) and $e^+e^- \rightarrow e^+e^-\gamma(ep)$ (dashed lines) at HERA
 A: $8^\circ < \theta_e < 172^\circ$
 B: $30^\circ < \theta_e < 150^\circ$
 C: $8^\circ < \theta_{e^+} < 172^\circ$
 D: $30^\circ < \theta_{e^+} < 150^\circ$
 Beam energies: $E_e = 30$ GeV
 $E_p = 820$ GeV

F. Le Diberder

The CELLO Collaboration has used high energy data ($38.3 < \sqrt{s} < 46.7$ GeV) taken in 1983-1985 to look for possible QED violations in the processes

$$e^+e^- \rightarrow \bar{l}l, \bar{l}l', \tau$$

where all four final state leptons are observed at large angles in the detector.

If the process is mediated by multiperipheral graphs (Fig. 12a) the experimental cuts correspond to very large Q^2 for the exchanged photons. However in this region of phase space other graphs such as bremsstrahlung (Fig. 12b), annihilation (Fig. 12c) and conversion (Fig. 12d) can give important contributions. The data was compared with a Monte Carlo event generator written by Berends, Daverveldt and Kleiss that takes into account all 36 'lowest order' diagrams belonging to the classes shown in Fig. 12.

The selection criteria demand 4 charged tracks with $p > 200$ MeV/c and $|\cos\theta| < 0.92$. All dilepton effective masses must be > 1 GeV/c². For the eeee and eeμμ samples further cuts are required:

- > 2 tracks with $|\cos\theta| < 0.6$
- 1 electron with $E > 2$ GeV/c
- 2 other identified (e,μ) with $p > 2$ GeV/c

Electrons are identified by their showering behaviour in the electromagnetic calorimeters, and muons by muon chamber hits. These cuts yield 8 eeμμ, 6 eeee and 1 eeττ candidates. In addition 1 μμμμ event is found by relaxing the electron requirement.

To search for QED violations using data with a range of different

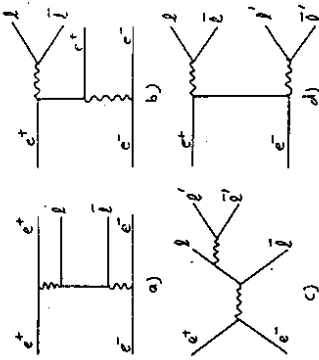


Fig. 12: Feynman diagrams contributing to the production of 4 lepton final states:
 a) Multiperipheral,
 b) Bremsstrahlung,
 c) Annihilation,
 d) Conversion graphs

the electromagnetic calorimeters, and muons by muon chamber hits. These cuts yield 8 eeμμ, 6 eeee and 1 eeττ candidates. In addition 1 μμμμ event is found by relaxing the electron requirement.

\sqrt{s} values a scaling parameter

$$x = \min \left\{ \frac{W_{ee}}{E_b}, \frac{W_{\mu\mu}}{E_b} \right\}$$

was defined, which is sensitive to possible QED violations at large mass scales (E_b = beam energy).

The distributions of x are shown for eeμμ, eeee respectively in Fig. 13a, b. The total integrated luminosity used is 52 pb^{-1} of which 27 pb^{-1} comes from 1985 (the corresponding entries are shaded in Fig. 13). The excess observed in the 1983-4 data¹⁴ for $x > 0.4$ in the eeμμ events is not confirmed in the 1985 data which alone is consistent with the Monte Carlo prediction (dashed histogram, absolute prediction for the full 52 pb^{-1} sample). However in the combined data sample there is still an excess for $x > 0.4$. Only time can tell if this is a large statistical fluctuation or a new physical effect.

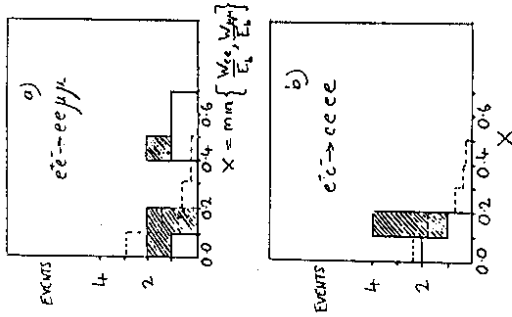


Fig. 13: Distributions of the x variable (see text) for a) eeττ, b) eeee final states. 1985 data is shaded. The dotted histogram is an absolute QED prediction for the total data sample (52 pb^{-1}) (CELLO).

A. Cordier

The new e^+e^- collider LEP now under construction at CERN provides a unique opportunity¹⁵⁻¹⁸ to investigate 2γ collisions in a so far unexplored energy domain. The beam energies and expected luminosities of some current and planned e^+e^- colliders are:

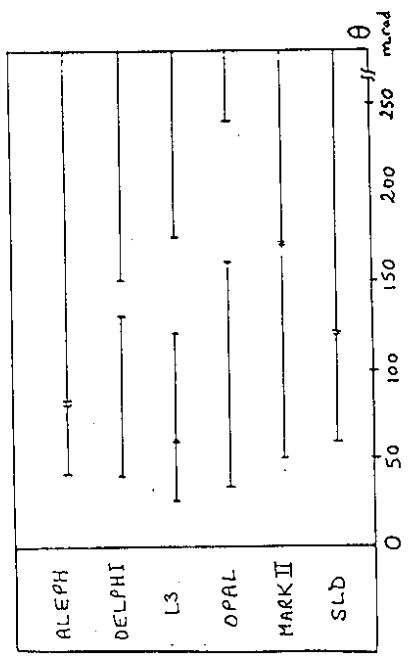


Fig. 15: Angular acceptances of the electron tagging systems of LEP and SLC detectors

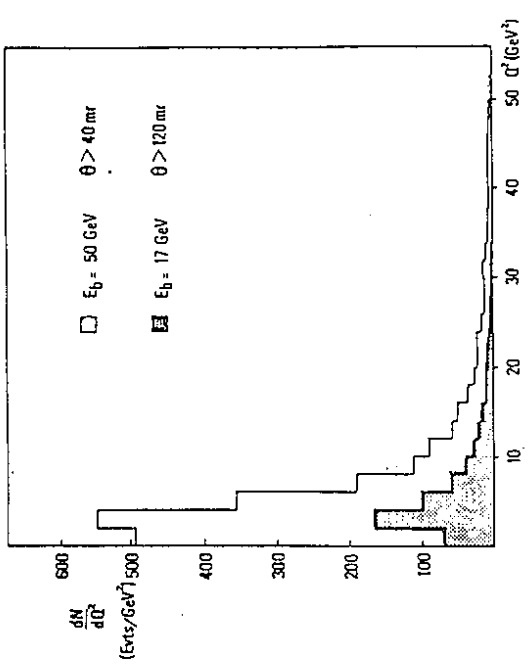


Fig. 16: dN/dQ^2 distributions for equivalent running time at PETRA (shaded) and LEP. Angular cuts are chosen so that $\langle Q^2 \rangle = 8$ (GeV/c) 2 .

E_b (GeV)	PETRA	SLC	LEP1/6	LEP2
	20	50	50	130
$L(10^{30} \text{ cm}^{-2} \text{ sec}^{-1})$	4	2	13	30

The effective luminosity for $\gamma\gamma$ physics as a function of W is shown in Fig. 14 for different colliders. The curves are corrected for acceptance ($10^\circ < \theta_{LAB} < 170^\circ$). For an isotropic CM angular distribution $\approx 70\%$ of produced particles are accepted by this cut.

As shown in Fig. 15 the planned LEP and SLC detectors have good coverage for electron tagging in the small angle region from $50 - 250$ mrad. Detection of the final state particles produced in $\gamma\gamma$ collisions will also be better than in general purpose detectors at PEP and PETRA (i.e. excluding the upgraded PLUTO and TPC 2 γ detectors). Typically final state particles will be accepted for $0 < \phi < 2\pi$ and $10^\circ < \theta < 170^\circ$. This leads to $W_{vis}/W_{true} \approx 0.85$ to be compared with ≈ 0.7 at PETRA thus enabling more precise unfolding of x_{true} from x_{vis} for structure function measurements.

LEP1/6 (50 GeV beam energy) is compared with PETRA for structure function measurements in Fig. 16, 17 which show, respectively, the Q^2 distribution and the W_{vis}^2 distribution for a typical LEP and PETRA detector. Different angular cuts are used for $E_b = 50, 17$ GeV so that in both cases $\langle Q^2 \rangle = 8$ (GeV/c) 2 . The advantages of LEP are apparent from these plots,

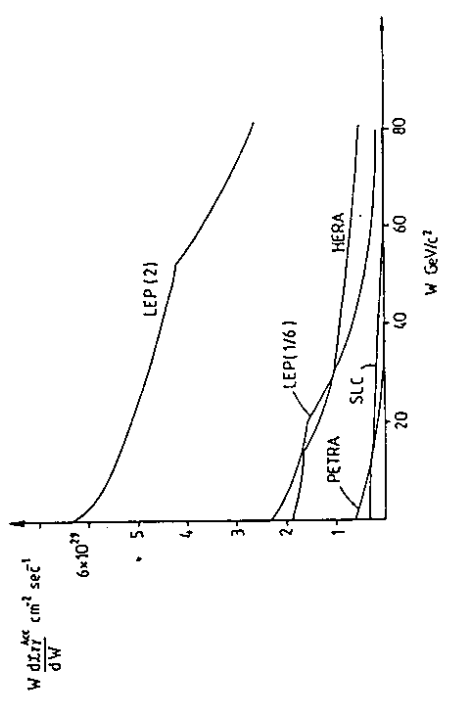


Fig. 14: Accepted differential $\gamma\gamma$ luminosity for various $e e$ and $e p$ colliders, as a function of the $\gamma\gamma$ C.M. energy W . An acceptance cut for the lab angular region $10^\circ < \theta < 170^\circ$ is applied.

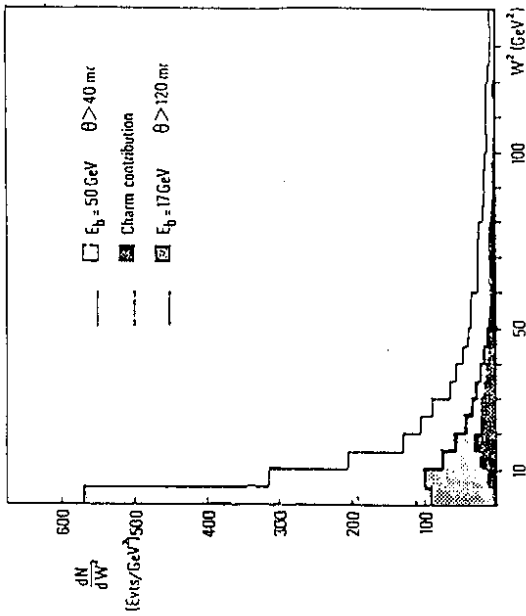


Fig. 17: dN/dW^2_{vis} distribution. Comments as for Fig. 16.

a large increase in the event rate at small W , Q^2 but tails in both distributions enabling measurement of F_2^Y at high Q^2 and detailed final state jet studies at high W^2 .

R.R. McNeil

A new measurement of the F_2 photon structure function in the low Q^2 region:

$$0.2 < Q^2 < 7 \text{ (GeV/c)}^2$$

has been made by the TPC 2 γ Collaboration.

A tagged electron with energy greater than 8 GeV in the angular range $28 < \theta < 180$ mrad is required corresponding to Q^2_{MIN} of 0.2 (GeV/c)^2 . An anti-tag constraint is applied in the opposite tagging arm to the detected electron, $E < 4 \text{ GeV}$ so that $p^2 < 0.1 \text{ (GeV/c)}^2$ for the target photon.

The hadronic final state is defined by the cuts:

- > 1 TPC Track
- > 2 Charged Tracks
- > 3 Particles (charged or neutral)
- > 1 Unambiguous Non-Electron in TPC
- $W_{vis} > 1 \text{ GeV}$

A loose cut requires p_T conservation:

$$\left| \sum p_T^{HADRON} + p_T^{TAG} \right| < 2 \text{ GeV/c}$$

and the total visible energy (including the tagged electron) is $< 0.8 \sqrt{s}$.

These cuts yielded 9200 events for an integrated luminosity of 50 pb^{-1} . Unfolded structure functions were obtained using the program of V. Blobel(20). The Monte Carlo used to describe the final state used a mixture of two different models:

Model A (Hadronic) The quarks are assumed to have a limited

$$p_T \text{ (with } \langle p_T \rangle = 300 \text{ MeV/c)} \text{ relative to the } YY^* \text{ axis}$$

Model B (Point-like) The quarks are distributed in angle as in the free quark parton model.

In both cases the quarks are fragmented into hadrons using the LUND program.

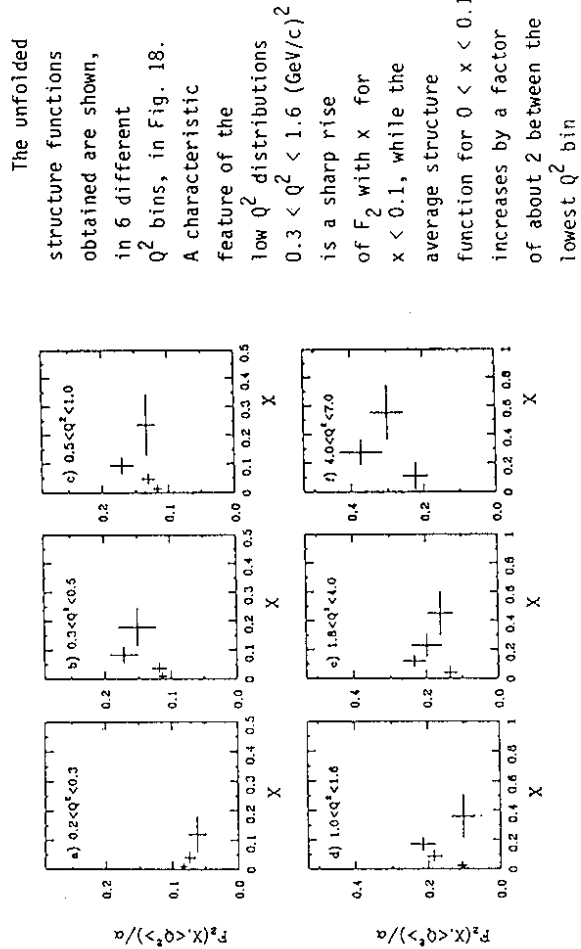


Fig. 18: The F_2 photon structure function versus x for different Q^2 intervals (TPC 2 γ)

The unfolded structure functions obtained are shown, in 6 different Q^2 bins, in Fig. 18. A characteristic feature of the low Q^2 distributions $0.3 < Q^2 < 1.6 \text{ (GeV/c)}^2$ is a sharp rise of F_2 with x for $x < 0.1$, while the average structure function for $0 < x < 0.1$ increases by a factor of about 2 between the lowest Q^2 bin

($0.2 < Q^2 < 0.3$) and the higher bins. From the relation:

$$F_2 = \frac{Q^2 \sigma_{\gamma\gamma}}{4\pi^2 \alpha}$$

it can be seen that at very low Q^2 values ($< m_p^2$) if $\sigma_{\gamma\gamma} = \text{const}$, F_2 is expected to decrease linearly with Q^2 . This can explain the rapid change observed for F_2 with Q^2 for $0 < x < 0.1$. The increase with x at constant Q^2 may also be explained by the behaviour of $\sigma_{\gamma\gamma}$. At small values of W , $\sigma_{\gamma\gamma}$ is expected to increase due to the effect of s channel resonances. If the cross section contains a piece $= \frac{1}{W^2}$, then for the corresponding structure function:

$$F_2 = \frac{Q^2}{W^2} = \frac{x}{1-x} = x \quad (x \text{ small})$$

This piece will then rise linearly with x at small x and be independent of Q^2 . At larger values of Q^2 the whole hadronic structure function is expected to be independent of Q^2 (Bjorken scaling). For larger values of Q^2 and x ($Q^2 > 1.8$, $x > 0.2$) the onset of the point-like component of the photon structure function is evident in Fig. 18.

The Q^2 dependence of F_2 for different x bins is shown in Fig. 19. For $0.0 < x < 0.1$ F_2 is independent of Q^2 , for $Q^2 > 0.3 \text{ GeV}^2$ which may be due to a combination of a large contribution from a $1/W^2$ term in the cross section at small Q^2 , W and the onset of the deep-inelastic region at higher Q^2 , W . In the higher x bins the point-like contribution can be clearly seen for $Q^2 > 4 \text{ (GeV/c)}^2$.

The three F_2 measurements shown in Fig. 18b, c, d are plotted together in Fig. 20. The three measurements are consistent with each other for all x values, and with the standard phenomenological parameterisation of the hadron structure function²¹⁾ for $x > 0.1$. This latter in turn agrees well with the directly measured pion structure function²²⁾. This first direct measurement of the hadronic photon structure function shows that it does indeed exist with the expected properties and so must be taken properly into account in any comparison of theory and experiment.

Finally the TPC 2 γ group performed an analysis of the final state jet structure. A sphericity axis was determined for each event, and the mean sphericity and the average p_T of a hadron relative to the sphericity

TPC/Two Gamma PRELIMINARY

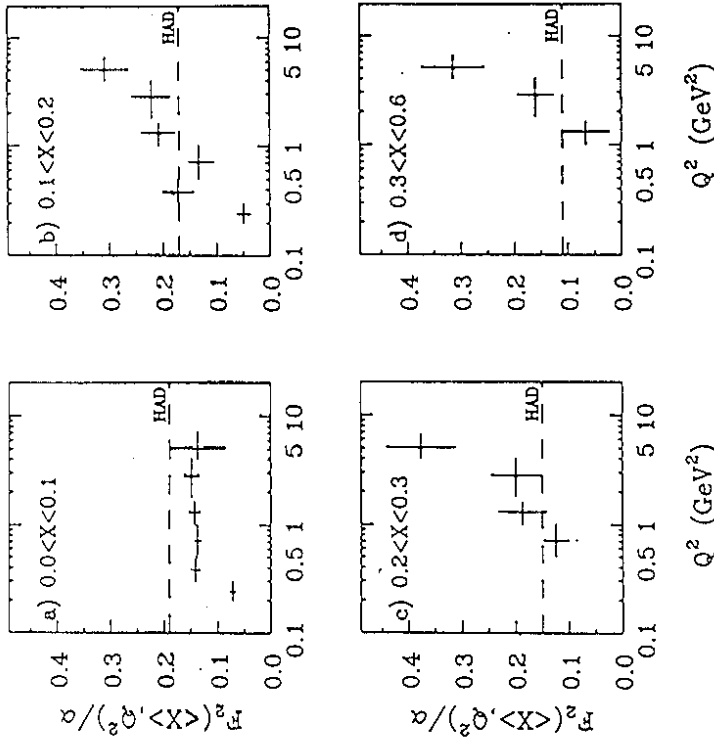


Fig. 19: The F_2 photon structure function versus Q^2 for different x intervals (TPC 2 γ)

TPC/Two Gamma PRELIMINARY

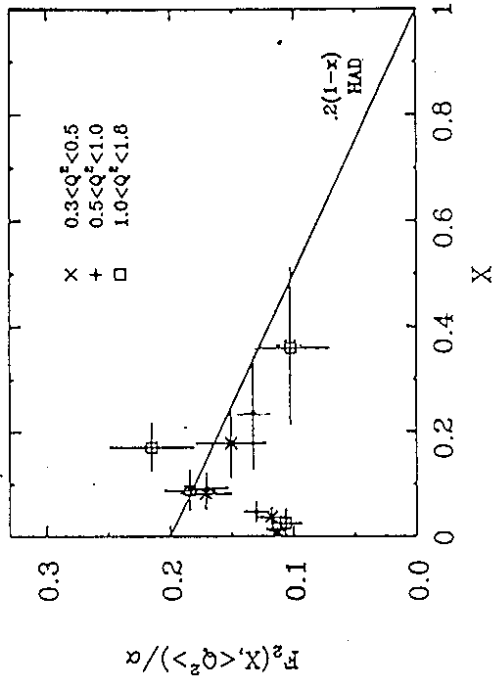


Fig. 20: First measurement of the hadronic F_2 photon structure function (TPC 2 γ)

axis were compared with Independent Phase Space (IPS) and 2-jet Monte Carlo predictions. The 2-jet model gives a good fit to the data, the IPS being excluded for $M_{vis} > 3 \text{ GeV}/c^2$.

The jet p_T^2 relative to the $\Upsilon\Upsilon^*$ axis is shown in Fig. 21 for various bands of Q^2 and x . The data is compared to the predictions of the models A, B defined above which in each case are shown separately, normalised to the total number of events. For small x , small Q^2 and $p_T^2 < 2 \text{ (GeV}/c)^2$ Model A gives a good fit. For small x and large Q^2 the data lie between the two models at large p_T^2 , whereas at large Q^2 and $x > 0.1$ the point-like model alone seems to give a satisfactory description. Fig. 22 shows the

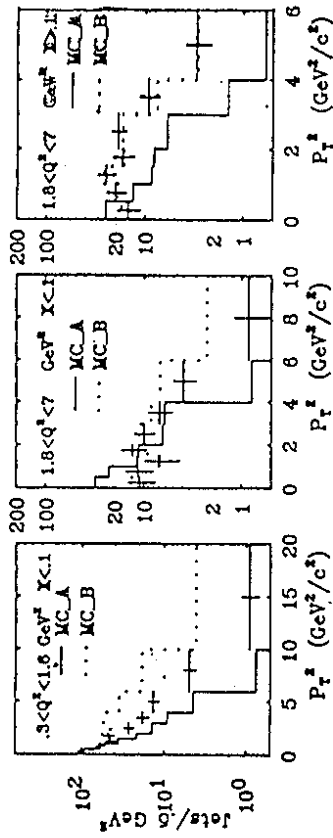


Fig. 21: Comparison of distributions of p_T^2 of final state jets relative to the $\Upsilon\Upsilon^*$ axis with different Monte Carlo models (TPC 2 γ)

results of fits to the jet p_T^2 distribution to the models A, B as a function of Q^2 and for two different x bins. The ordinate is the percentage of model A in the fit. For the x_{vis} interval $0.0 < x_{vis} < 0.1$ the ratio is $\approx 50\%$ almost independent of Q^2 , whereas for $0.1 < x_{vis} < 0.42$ the fit is consistent with model B only. This result is suggestive, however it is clear from Fig. 20 that the hadronic structure function is not expected to vanish for $x > 0.1$ and that some point-like contribution is expected, even at small x values as Q^2 increases. The error bars in Fig. 22 are sufficiently large to accommodate both of these effects.

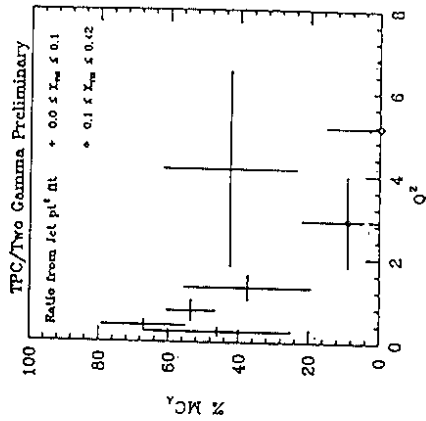


Fig. 22: Percentage of model A (VMD, hadronic F_2) fit fitted to the p_T^2 distribution of final state jets, versus Q^2 , for different x intervals (TPC 2 γ)

References

- 1) See talk of B. Shen in these proceedings
- 2) D.M. Binnie et al., Phys.Lett. 83B (1979), 141
- 3) J.E. Olsson in Proceedings of the Fifth International Workshop on Photon Photon Collisions, Aachen 1983.
Lecture Notes in Physics 191, Springer Verlag, Ed. Ch. Berger
- 4) Ch. Berger et al. (PLUTO Collaboration), Phys.Lett. 167B (1986), 120
- 5) CERN pre-print CERN EP/EL-0027P (1984)
- 6) See talk of A. Falvard in these proceedings
- 7) See talk of J. Smith in these proceedings
- 8) G.R. Farrar in Proceedings of the Sixth International Workshop on Photon Photon Collisions, Lake Tahoe 1984.
World Scientific Singapore, Ed. R.L. Lander
- 9) M. Althoff et al. (TASSO Collaboration), Phys.Lett. 130B (1983), 449
- 10) A. Courau, Phys.Lett. 151B (1985), 469
- 11) A. Courau, Phys.Rev. D29 (1984), 24
- 12) A. Courau and P. Kessler, Orsay pre-print LAL 85-06,
College de France pre-print LPC 85-05
- 13) H.-J. Behrend et al. (CELLO Collaboration), Phys.Lett. 168B (1986), 420
- 14) H.-J. Behrend et al., DESY pre-print 84-103 (1984)
- 15) J.H. Field in Proceedings of the International Workshop on $\Upsilon\Upsilon$ Collisions, Amiens, France 1980.
Lecture Notes in Physics 134, Springer Verlag, Ed. G. Cochar and P. Kessler
- 16) M. Davier in Proceedings of the Fourth International Colloquium on Photon Photon Interactions, Paris 1981.
World Scientific Singapore, Ed. Georges W. London
- 17) A. Cordier, "Measurement of the F_2 Photon Structure Function at LEP", Orsay pre-print LAL 85/35, September 1985
- 18) A. Ali, "QCD, $\Upsilon\Upsilon$ and Heavy Quark Physics at LEP", DESY 86-032, March 1986
- 19) J.H. Field in Proceedings of the Fifth International Workshop on Photon Photon Collisions, Aachen 1983.
Lecture Notes in Physics 191, Springer Verlag, Ed. Ch. Berger
- 20) See for example A. Bäcker in Proceedings of the Sixth International Workshop on Photon Photon Collisions, Lake Tahoe 1984.
World Scientific Singapore, Ed. R.L. Lander
- 21) C. Peterson, T.F. Walsh and P.M. Zerwas, Nucl.Phys. B229 (1983), 301
- 22) J. Badier et al., Z. für Physik (Particles and Fields) C18 (1983), 281

DISCUSSION

Q. - Brodsky

Could you comment on the status of the $\Upsilon\Upsilon \rightarrow \pi^+\pi^-$ enhancement near threshold from other experiments?

A. - J.H. Field

The published PLUTO data (Ch. Berger et al., Z. für Physik C26 (1984), 199) also shows a large excess over the Born term prediction for $\pi\pi$ masses around 400 MeV/c². The Crystal Ball Collaboration at DORIS is currently analysing the related channel $\Upsilon\Upsilon \rightarrow \pi^0\pi^0$ in the same mass region.

Q. - Kolanoski

1) Remark: The JADE and MARK J. Collaborations analysed also the 4 lepton final state. Both find agreement with QED.

2) How much time did DM2 spend on the $\Upsilon\Upsilon$ experiments? Is it possible to enlarge the data sample?

A. - J.H. Field

The DM2 data was taken in September-October 1982. The DM2 detector has now been dismantled, so there is no possibility of increasing the data sample.